

Chapter 2

Porosity, Pore Size Distribution, Micro-structure

Mike Lawrence and Yunhong Jiang

Abstract The high porosity and microstructure of bio-aggregates are fundamental to their physical properties. Typically they have a low density and a complex pore structure. This has two principal effects. In the first instance, low density is associated with low strength, but also with low thermal conductivity. For this reason most bio-aggregates are not suitable for use as structural materials, but are eminently suited to act as a low density filler in composite materials conferring low thermal conductivity on the resulting bio-composite. The complex nature of their porosity results in a material that is able to readily adsorb moisture and humidity. This results in a material that has an exceptionally high moisture buffering capacity, a characteristic that is of great interest in building materials, because it tends to stabilise the internal environment of a building, thereby resulting in a much more healthy indoor environment. This chapter considers the range of methods that can be used to measure porosity and to characterise the microstructure of materials in general, and discusses how some of these techniques have been used on bio-aggregates. It also identifies opportunities to use novel techniques on bio-aggregates in order to improve our understanding of their porosity, pore size distribution, pore connectivity and microstructure, all of which are characteristics that are essential to the optimisation of the performance of bio-aggregates within the construction industry.

Keywords Porosity · Microstructure · Physisorption · Mercury Intrusion Porosimetry · Scanning Electron Microscopy · X-Ray Computed Tomography

M. Lawrence (✉) · Y. Jiang
BRE Centre for Innovative Construction Materials, University of Bath,
Bath BA2 7AY, UK
e-mail: m.lawrence@bath.ac.uk

© RILEM 2017
S. Amziane and F. Collet (eds.), *Bio-aggregates Based Building Materials*,
RILEM State-of-the-Art Reports 23, DOI 10.1007/978-94-024-1031-0_2

2.1 Introduction

Porosity is a measure of the void fraction in a material. Voids can either be ‘closed’, and inaccessible or ‘open’ and connected to other voids and thence to the exterior of the material. The total porosity (ϕ) is defined by the ratio of the volume of void space (V_V) to the total, or bulk volume of the material (V_T):

$$\phi = \frac{V_V}{V_T}$$

Porosity can also be expressed as a percentage of the bulk volume of the material. In bio-aggregates the pores are formed during the growth phase of the plant and in the living plant they have the function of nutrient storage and transmission of water and nutrients from the roots to the rest of the plant. Plant stems have a low density of between 110 and 120 kg.m⁻³ and a high porosity of the order of 70–80%. The specific properties of bio-aggregates, such as low density, high porosity and the complexity of pore size and pore structure, result in a material that has a low thermal conductivity, and which is highly absorbent, capable of absorbing up to four times its own weight in water. Once the shiv has been dried out it has a high moisture buffer value, conferring on it the ability to passively manage internal humidity levels when used as a building material (Latif et al. 2015).

Porosity is a rather easy parameter to define, but certainly not so easy to quantify. The reason is that the void/space in bio-aggregates can span from few nanometres to centimetres or larger. There is really no one method that can adequately cover this enormous range in scale. In addition, the porosity can be modified or changed by a variety of processes during the test such as deformation, hydrothermal alteration and producing secondary or fracture porosity. Finally, the pore shape and connection structure (open and closed) have a significant effect on the porosity results depending on the testing approach (Bismarck 2002; Brewer 2014; Chundawat 2011; Collet 2008; Donato 2012; Hamdi 2015; Dougal et al. 2006). The aims of this chapter is to summarize many of the available techniques that can be used to analyse the porosity of bio-aggregate materials. Manger et al. (1963) concluded that most of the total porosity measurements are variations on bulk volume/grain volume or bulk density/grain density approaches, and the apparent porosity measurements are made by variations of absorption methods for different fluids or gases. Anovitz et al. (2015) summarized 10 methods for measuring the porosity and pore size distribution (PSD) used on core or crushed rock materials (Fig. 2.1). This shows the range of pore sizes that each method is capable of measuring. It should be kept in mind that different techniques are based on different principles and have different capability for measurement. Depending on the natural properties of bio-aggregates, there is no best approach to determine their

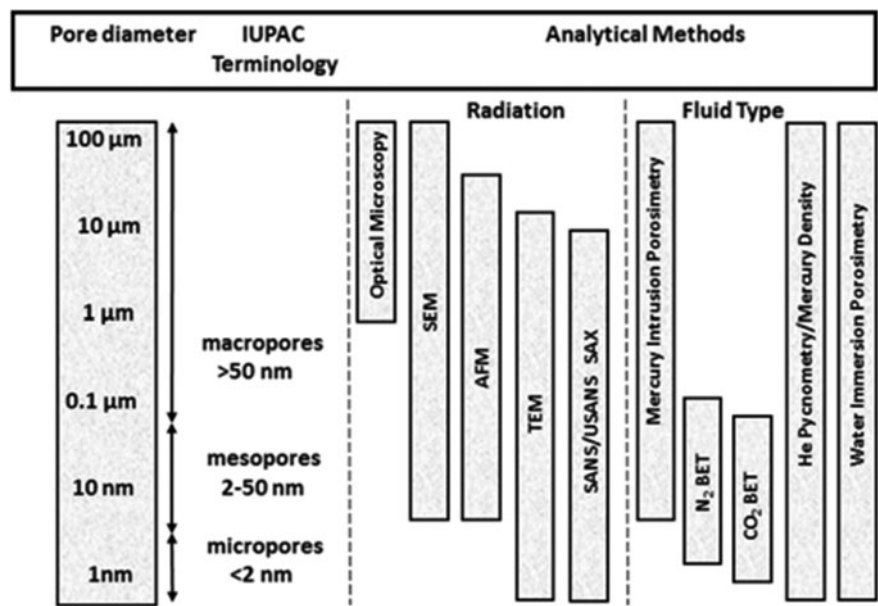


Fig. 2.1 Methods used to determine porosity and pore size distribution (PSD) (Anovitz and Cole 2015)

porosity. The combination of several techniques and comparing the results of pore structure from different methods may gain an insight into the complex pore system of bio-aggregates.

2.2 Techniques Used to Measure Porosity

2.2.1 Imaging Methods

With the development of digital images and computer software, image processing is a new and convenient method which is able to determine the pore size, pore size distribution, porosity and microstructure of bio-aggregates. There has been much progress in materials science, biology, and geology regarding the application of image analyse. It has become an important technique for the investigation of the porosity and particle size of bio-aggregates and bio-composites (Mermut et al. 2009; Ziel et al. 2008; Nimmo et al. 2004; Aydilek et al. 2002; Shen 2015). A broad range of imaging methods are available to describe the nature of porosity in bio-aggregates materials. 2D techniques that can be used include: optical light microscopy (OM), scanning electron microscopy (SEM) with energy dispersive X-ray spectroscopy (EDX), field emission scanning electron microscopy (FESEM),

focused ion beam (FIB), transmission electron microscopy (TEM). The range of 3D techniques available include: nuclear magnetic resonance (NMR), atomic force microscopy (AFM) and X-ray tomography (Anovitz et al. 2015). Based on the images of samples, computer image processing can be considered as an additional method of sample analysis. There are a wide range of image processing software available to analyse images, including ImageJ, MATLAB, ICY, Avizo, Image Pro and others (Grove et al. 2011; Yang et al. 2014). 2D image analysis allows the measurement of parameters such as pore or particle shape, pore or particle size and size distribution, spatial distribution of particles, and also the corresponding measurements for vesicles. With the use of stereology and/or 3D texture models, it is possible to investigate the meaning of these 2D measurements in the 3D volume. The 3D image analysis provides a direct way of testing the 3D particle/pore size measurements using X-ray tomography. Dougal et al. (2006) summarized the features and limitations of 2D and 3D image analysis method (Fig. 2.2).

2.2.1.1 Optical Microscopy

Optical Microscopy has been used since the 17th century when it was first used by Robert Hooke to describe ‘...minute bodies made by magnifying glasses with observations and inquiries thereupon.’ Since that time the optical microscope has been refined to produce the range of modern research microscopes used in laboratories today.

Transmitted Light Microscopy uses light that is transmitted from a source on the opposite side of the specimen to the objective lens. Normally the light is passed through a condenser to focus it on the specimen in order to maximise the amount of light available. The optimum set-up for specimen illumination and image generation is known as Köhler illumination after the man who invented it. It is used for most of the optical configurations listed below. The microscope techniques requiring a transmitted light path include bright field, dark field, phase contrast, polarisation and differential interference contrast optics. Transmitted light microscopy relies on preparing samples that are sufficiently thin to allow the passage of light. Some materials remain opaque even when ground to a thickness of 30 μm , and for this reason reflected light microscopes have been developed. The sample is often polished to a high degree in order to allow all the features to be seen in the same plane, and therefore remain in focus. Samples are illuminated from above through the objective.

Bright Field Microscopy is the most frequently used technique where no optical contrast methods are used. It uses transmitted light to view a specimen that contains inherent contrast or where the specimen has been stained to improve contrast. Figure 2.3 shows a transverse section of Hemp shiv that has been set in a blue stained resin under a $\times 10$ magnification and Fig. 2.4 shows the central section of the same specimen under $\times 40$ magnification.

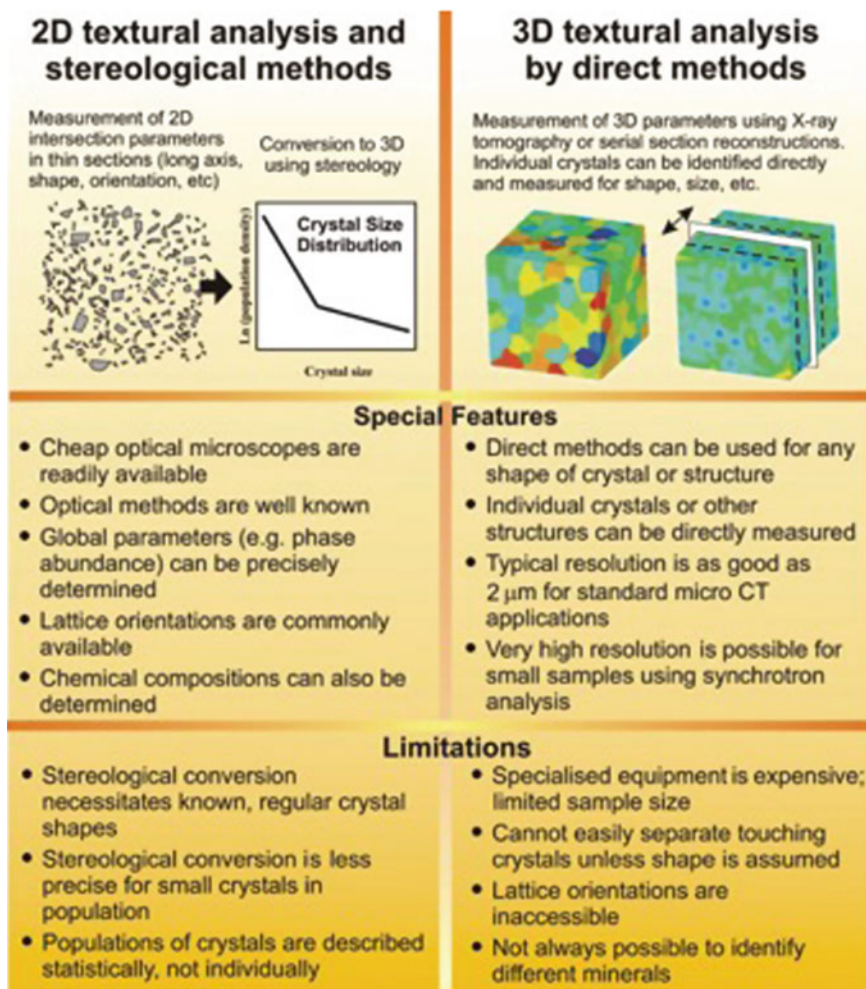


Fig. 2.2 Comparison of the imaging analysis approaches in 2D and 3D analysis (Dougal et al. 2006)

Dark Field Microscopy uses oblique illumination, and is used for the detection of micro-organisms in unstained smear preparations and diatom studies. Phase contrast exploits the phenomenon that light slows slightly when passing through biological specimens. When used in conjunction with phase contrast objective lenses which contain a corresponding phase plate, degrees of constructive and destructive interference occur which produce the characteristic light and dark features in the image.

Polarised Light Microscopy uses plane polarised light to analyse structures that are birefringent, which is to say structures that have two different refractive indices

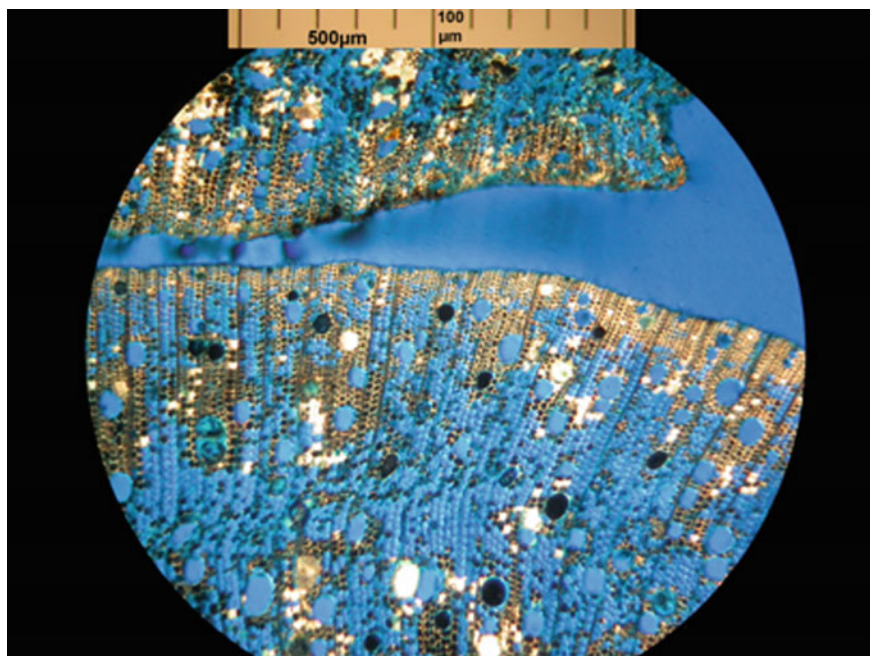


Fig. 2.3 Cross-section of hemp shiv $\times 10$ (author)

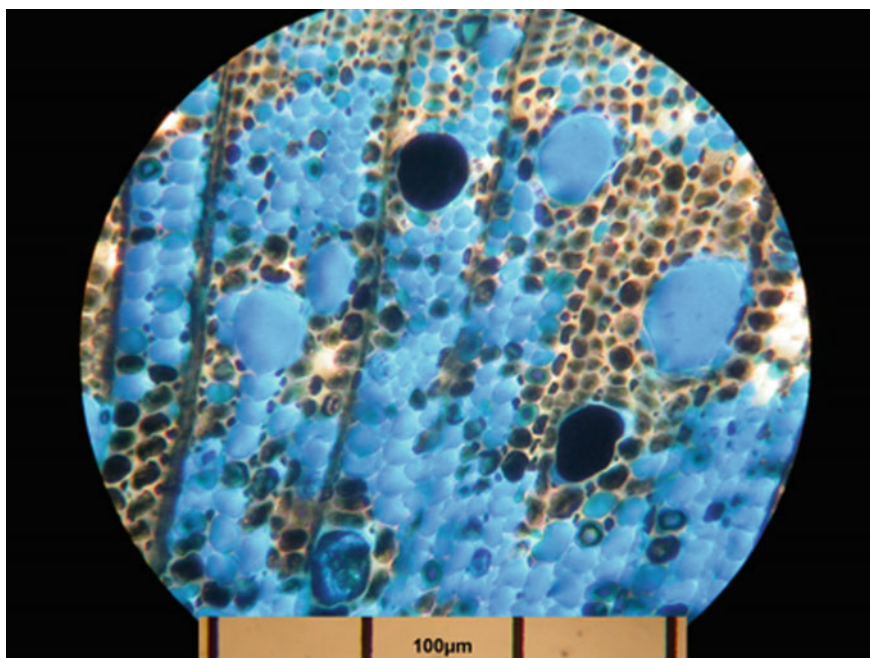


Fig. 2.4 Cross-section of hemp shiv $\times 40$ (author)



Fig. 2.5 Transverse section of hemp-lime in light polarised at 0° (*left*) and 90° (*right*) (author)

at right angles to each other (e.g. calcite). Figure 2.5 shows a transverse section of hemp-lime in light polarised at 0° (*left*) and 90° (*right*). This clearly shows the coating of lime binder around the bio-aggregate and demonstrates that the binder has only limited penetration into the capillaries of the material.

Differential Interference Contrast Microscopy is a more complex form of polarised light microscopy involving two slightly separate plane polarised beams of light to create a 3D-like image with shade of grey.

Stevulova et al. (2014) used reflected light microscopy to examine the surface morphology of hemp shiv and the impact of different surface treatments (Fig. 2.6).

2.2.1.2 Scanning Electron Microscopy

Scanning Electron Microscopy (SEM) is one of the most popular imaging techniques. Porosity can be measured by image analysis based on scanning electron microscopy incorporating digital image processing. In addition, the dimension, shape and the number of pores in bio-aggregates and bio-composites can be inspected by image processing analysis. The image analysis was developed using various mathematical morphology algorithms to provide a complete pore size distribution (PSD) curve for each sample. The main image processing tasks are sample preparation, specimen scanning process, image enhancement, pixel classification, and pixel clustering (Kaestner et al. 2008; Dougal et al. 2007). The key to be able to perform accurate digital porosity measurements is the ability to generate a porosity threshold image (one which separates the porosity voids from the rest of the objects in the image). The signals of the secondary electrons gives information on the surface topography. The backscattered electrons (BSE) gives complementary information of the chemical composition of the sample surface. High atomic number elements backscatter electrons more strongly than low atomic number elements, and thus appear brighter in an image. BSE are used to detect contrast

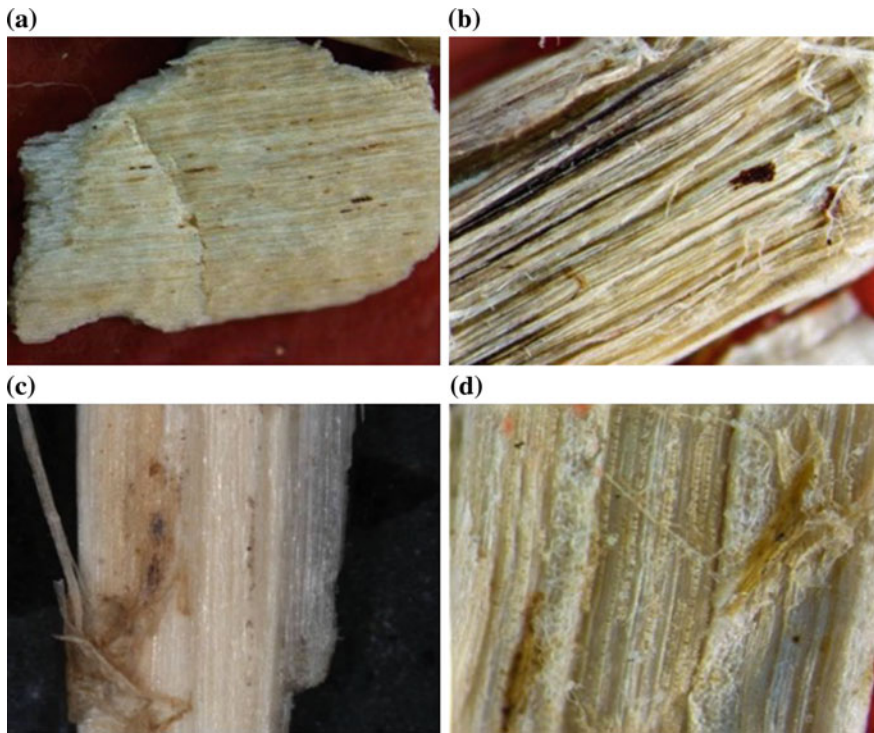


Fig. 2.6 Micrographs of original sample of hemp hurds (a) and chemically modified by NaOH (b), EDTA (c) and Ca(OH)₂ (d) (40× magnification) (Stevulova et al. 2014)

between areas on the sample surface with different chemical compositions. In a backscattering electron image, the relative difference between signals, known as the contrast, C , can be obtained from the following equation:

$$C = \frac{\eta_1 - \eta_2}{\eta_1}$$

In which η_1 and η_2 are, respectively, the backscattering coefficients for high and low density materials. The minimum value of C in an image is defined by the threshold equation:

$$i_B > \frac{4 \times 10^{-12}}{\epsilon C^2 t_f}$$

In which i_B is the minimum beam current required to provide contrast C , t_f is the time required to scan a 1000×1000 pixel frame (typical SEM pixel density for a

photomicrograph), and ϵ is the detector “efficiency” (ratio of signal current to beam current). The ultimate resolution available with SEM is on the order of $0.5\ \mu\text{m}$ (Zhao et al. 1992).

There are many factors affecting the calculated results, such as the thin section thickness, threshold value, and pore circularity (Anovitz et al. 2015; Marinello et al. 2008). Poor quality data can arise from the introduction of noise and inadequate or overzealous pre-processing methods, increasing user bias during thresholding. The kind of sample preparation required of the sample depends on whether it is electrically conducting or not. Non-conductive samples must first be sputter coated with an ultra-thin coating of an electrically-conducting material before imaging. Otherwise, samples will tend to charge when scanned by the electron beam leading to scanning faults and other image artifacts. The advantages of the SEM over optical petrography are greater depth of field and resolution, and a significantly higher magnification range. It can provide direct and detailed structural information including the shape and size of individual pore inside the bio-aggregates. The assumptions about pore shape are not made, but rather images capture this information directly. The disadvantage of SEM is that the obtained images are exactly two-dimensional grey scale image. The SEM images showed partly the inner structure of the samples and they cannot be considered completely as sections. It underestimates the pore radius due to only working part of the pore. However, Image-based analyses have been used to extract meaningful quantities which characterize pore structure and describe several spatial characteristics of porosity. Mathematical correction techniques are necessary to estimate unbiased pore body and opening sizes. Sizing techniques, a two-point correlation technique, and fractal analysis can be used to analysis the individual pore size, shape and distribution (Zhao et al. 1992).

During the past ten years, SEM image analysis has become an important tool for microscopic studies of bio-aggregates based materials. SEM images have been used to study aspects of bio-aggregates porosity by several researchers. Walker and Pavia (2014) studied the microstructure and pore size of hemp lime concrete using FESEM. The results showed that the morphology of hemp interface changed over time, from predominantly needle-shape at early ages to sponge and gel types at later ages. A wide distribution of pore size was evident in all binders. Most pores ranged from 200 to 2000 nm. Lubelli et al. (2013) studied porosity and pore size distribution of a wet poultice by using a FIB-SEM with a cold stage and MIP. The incremental and cumulative pore diameter distribution obtained using cryo-SEM image method showed the prevalence of pore radii in the range of 100 nm. The total pore fraction varies between 26 and 44% and the mean pore radius between 110 and 160 nm. The total pore area obtained by image analysis was 44%, which is significantly smaller than the total pore volume measured by MIP (57.93%). This is might be due to the absence of pores diameter larger than $1.2\ \mu\text{m}$ in the studied cryo-SEM images (Lubelli et al. 2013). Chundawat et al. (2011) studied the shape, size (10–1000 nm), and spatial distribution of the pores on their location within the cell wall and the cell wall volume, ranged between 0.005 and $0.05\ \text{nm}^2$ per nm^3 by

using TEM-image analysis. Figure 2.7 showed how water was likely incorporated in additional hydrates resulting in weight gain (7 wt%) of the hemp-lime concrete and abundant needle shaped hydrates are growing into the pores suggesting a reduction in pore size (Walker 2014).

There are a large number of papers which discuss SEM image analysis approaches to the analysis of the pore size distribution and pore shape of soil and membrane materials. However, there only few papers that use the SEM image analysis method to study porosity and pore distribution on bio-aggregates. Sassoni et al. (2014) have used SEM to visualise the microstructure of bio-aggregate composites (Fig. 2.8), but did not use the information to analyse the pore structure or pore size distribution.

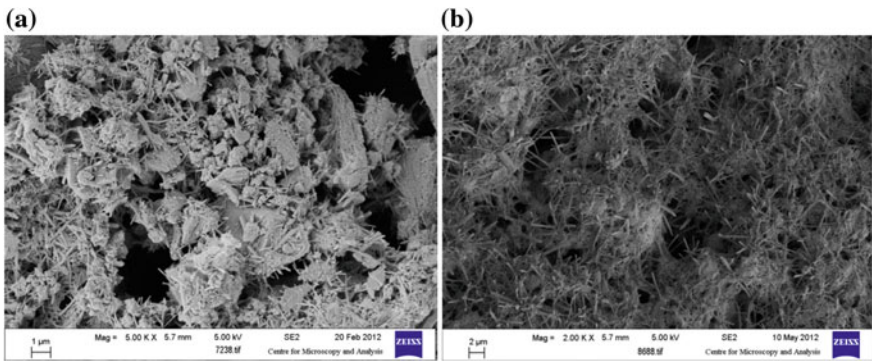


Fig. 2.7 Hydrates in hemp lime concrete made with commercial binder (a) and in-creased quantity of hydrates in the binder of hemp concrete saturated with water for 2 weeks (Walker et al. 2014)

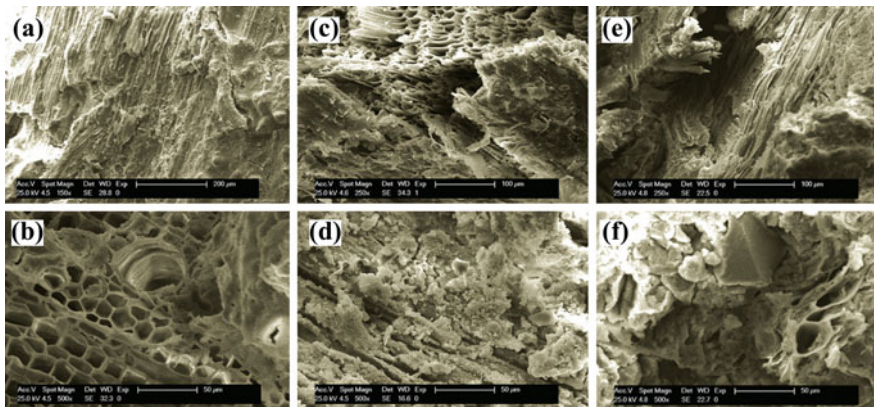


Fig. 2.8 Visualisation of the microstructure of low density (a and b), medium density (c and d) and high density (e and f) hemp shiv-magnesium oxide composites (Sassoni et al. 2014)

The SEM image analysis methods demonstrate the ability to quantify the nature of porosity in complex heterogeneous matrices. In the bio-aggregates, there is a hierarchy of pore types that range from micro-pore to organic meso-pore to fracture macro-pores. For future experimental work, SEM image analysis approach will be an important technique for analysing the porosity of bio-aggregate materials.

2.2.1.3 X-Ray Computed Tomography

X-ray computed tomography (XRCT) has been used to characterize the cellular microstructure and porosity of bio-aggregates materials. This method can produce the non-destructive and three-dimensional images to quantify the micro-structure such as pore size distribution, porosity and tortuosity of the porous network. X-ray radiography physics is based on the Beer-Lambert law (Maire et al. 2001; Dougal et al. 2007; Roche et al. 2010). Pore are distinguished in X-XRCT on the basis of their linear attenuation coefficient, μ . This parameter depends on the electron density of the sample, the effective atomic number of the sample, and the energy of the incoming X-ray beam. XRCT comprises an X-ray source, a rotation state on which the object is fixed, an X-ray detector and a reconstruction software (Dougal et al. 2007). Construction of a 3D map of a specimen, several X-ray radiographs of the sample are recorded at different viewing angles. This imaging information is then used in reconstruction software to recalculate the 3D map of the attenuation from the combination of the obtained radiographs. The Fig. 2.9 shows the stages from image capture through to processing and finally to reconstructed 3D virtual texture ready for quantification. The crucial point in applying tomography to materials science is the achievable spatial resolution. For a limit resolution of the order of 8 μm , a cone-beam system can be used with a classical micro-focus X-ray tube as the source. Most recent lab systems routinely achieve resolution as low as 5 μm . Larger samples have a lower resolution, limited by the number of pixels. The best quality images in terms of signal-to-noise ratio and spatial resolution allowing high-resolution micro-tomography are obtained on synchrotron radiation (Maire et al. 2012).

There are several disadvantages about XRCT porosity analysis. These include: 3D methods are not always applicable if samples are too large or small; it is very expensive and cannot distinguish touching grains of the same mineral; nor can it clearly separate different minerals with very similar properties.

Mostefai et al. (2015) investigated microstructural effects of hemp fibre and shiv addition on modified mortars by using X-ray tomography. Results showed that porosity level in hemp shiv modified mortar with regard to the weight content of 2 wt%, is 5.08%; whereas, porosity in the case of hemp fibre modified mortar is 3.54%. Both of hemp filler play a significant role in triggering the porosity content. The porosity of wood bark insulation board was studied by using XRCT

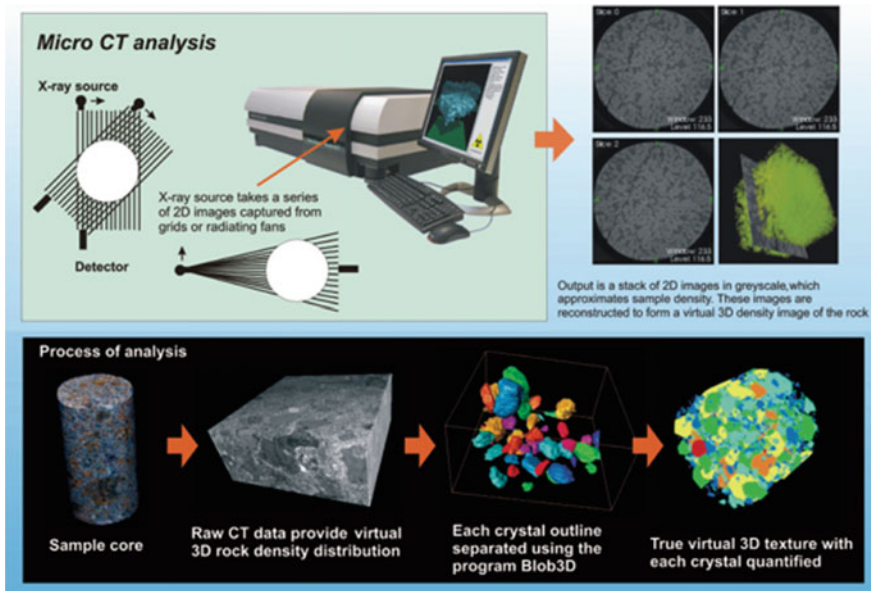


Fig. 2.9 Measuring 3D textures using XRCT techniques. X-rays are passed through the sample to produce a series of 2D images that are spaced close to each other (typically at resolutions of 7–30 μm). Sequential images are captured by rotating the sample or source. Using software such as Blob3D, the individual elements of the texture, such as crystals, can be sampled and quantified (Douglass et al. 2007)

(Fig. 2.10). The results showed that pore size distribution is clearly influenced by the panel density and the small pores ($<1 \text{ mm}^2$) are predominantly pores within the bark materials itself. In addition, larger pores ($>1 \text{ mm}^2$) are void due to imperfect stacking during the press process.

Pores smaller than 1 mm^2 account for between 8 and 30% of the pore area (Kain et al. 2015). William et al. (2015) studied the volumetric ratios change of visible air voids related to consolidation process in the level of macro scale by using XRCT. The results showed that the ratio of macro scale air voids to micro scale air voids changed significantly during the consolidating process. Hamdi et al. (2015) studied and compared the X-ray computed tomography and 2D image analysis on lignocellulosic fibres raw materials. The strengths and drawbacks of the applied imaging methods on lignocellulosic materials are listed in Table 2.1.

Tran et al. (2015) studied the porosity of coir fibre by using SEM image analysis and XRCT analysis. The results from SEM methods with software Leica QWin showed that the fibre porosity is in the range from 22 to 30% (Fig. 2.11). In reality, the lumen of each elementary fibre is not a cylinder. In this case, the volume of lumens can be underestimated when a smaller cross section is analysed. The porosity of the coir fibres using XRCT methods, ranges from 27 to 40%. The fibre

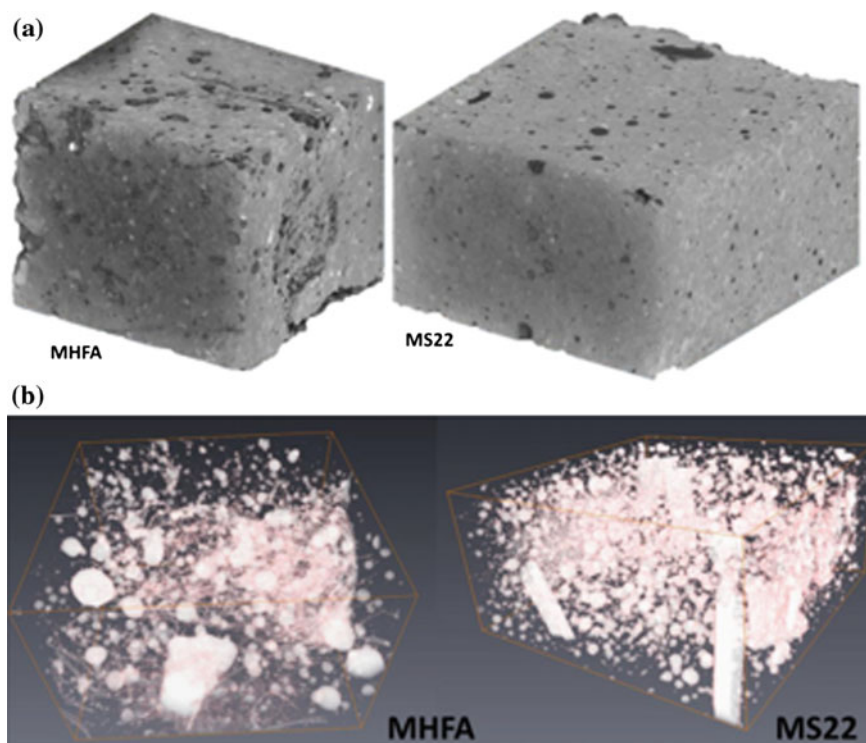


Fig. 2.10 **a** X-ray μ -tomography images of hemp fibre (MHFA) and shiv (MS22) modified mortars. Representative dimensions are $26 \text{ \AA} \sim 22 \text{ \AA} \sim 21 \text{ mm}^3$ and $37 \text{ \AA} \sim 38 \text{ \AA} \sim 22 \text{ mm}^3$ for MHFA and MS22, respectively. **b** In-depth views showing porosity and hemp phase arrangement. Crop volumes are $24 \text{ \AA} \sim 21 \text{ \AA} \sim 16 \text{ mm}^3$ and $38 \text{ \AA} \sim 38 \text{ \AA} \sim 19 \text{ mm}^3$ for MHFA and MS22, respectively (Mostefai et al. 2015)

porosity analysed with this method is likely to be overestimated because the method is based on the densitometry principle, and there is only a small difference in density between coir fibres and air. In addition, coir fibres consist of various thin organic tissues, which may not be detected on the scanned images. The author concluded that Image analysis on SEM pictures will give a better estimation of the porosity of coir fibres.

In summary, XRCT offers a good tool to study the porosity and generally the internal structure of bio-aggregates. Based on the above discussion, the bio-aggregate porosity will be better estimated by SEM image analysis in a small level of scale ($<1 \text{ }\mu\text{m}$). XRCT will give a better results on the porosity of bio-aggregate above $1\text{--}3 \text{ }\mu\text{m}$. Combining these two methods will improve accuracy of pore-size distributions and porosity for bio-aggregates.

Table 2.1 Characteristics of the X-ray CT and 2D scanning methods for lignocellulosic fibre size estimation

Imaging technique	Strengths	Drawbacks
X-ray CT	<ul style="list-style-type: none">– Suitable for the detection of small fiber entities– High level of detail and ability to internally observe the structures– Reliable fiber size estimation for regular shapes with low rates of porosity and small amounts of large bundles– Does not reject fiber size estimation of hollow fibers (which can be filled)	<ul style="list-style-type: none">– Fibers with a length greater than the maximum 3D Spatial resolution of X-ray microtomograph cannot be assessed– Fibers with a diameter smaller than the minimum 3D Spatial resolution of the X-ray microtomograph cannot be assessed– Underestimates the fiber size distribution of a heterogeneous fiber elements
2D scanning	<ul style="list-style-type: none">– Reliable fiber size estimation for regular fiber shapes with low rates of porosity and small amounts of large bundles– Relatively easy implementation and high reproductibility	<ul style="list-style-type: none">– Exponentially overestimates the fiber size distribution of heterogeneous fiber population with a high porosity level– Underestimates the fiber length distribution of heterogeneous fiber network with high rates of tortuosity– The fibers need to be manually spread over the scanner surface to prevent inter-fiber contacts

Hamdi et al. (2015)

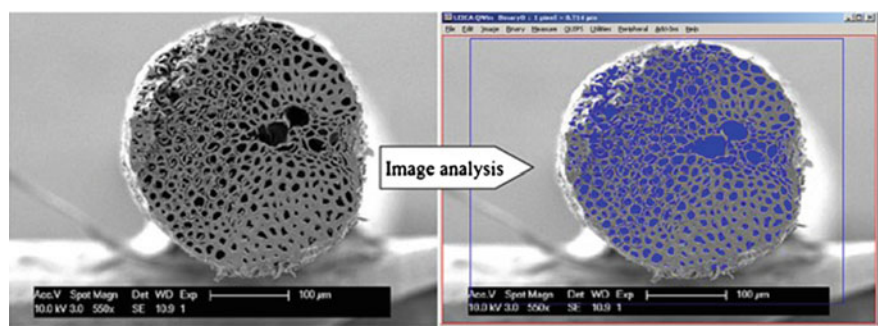


Fig. 2.11 Image analysis to measure the porous area of the fibre cross-section using the software Leica QWin (Tran et al. 2015)

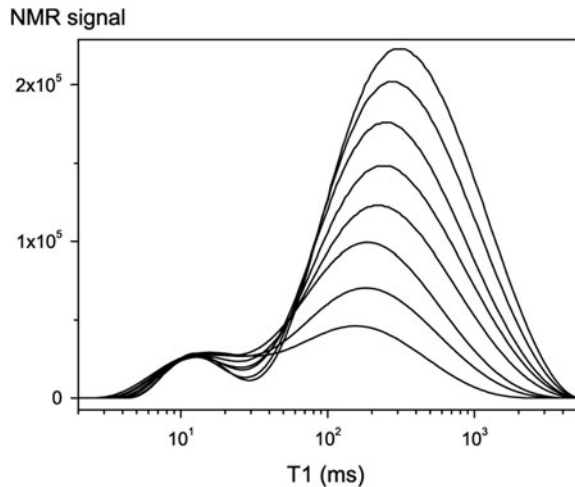
2.2.1.4 Nuclear Magnetic Resonance

NMR Spectroscopy has been used commercially in a variety of disciplines, ranging from oil exploration to food technology, to examine the moisture content of materials. The hydrogen atoms within the material, which is exposed to a large

magnetic field, are excited by a pulse of radio waves, and subsequently relax back to their normal state releasing a characteristic signal. Measurement of the relaxation signal (T_1) allows the number of hydrogen atoms present and, with appropriate calibration for the material, the absolute water content to be evaluated. An additional feature of NMR is its ability to measure the amount of moisture in different physical states (i.e. chemically bound, physically bound and free liquid). Because the technique is tuned to excite the hydrogen nucleus, water molecules are particularly responsive to the technique, however, care is needed where polymer-based or organic materials are present as their hydrogen content may confuse results. The technique requires experience and sophisticated analysis to fulfil its potential performance (Phillipson et al. 2007).

Faure et al. (2012) investigated water transfer in hemp-lime using NMR. The relaxation time T_1 is known to be a probe of water mobility which depends on the water interaction with its environmental conditions: ions or paramagnetic components, media rigidity (for example due to polymer presence), pore size, etc. In complex media such as civil engineering materials, water present in the sample may experience different local environment: it may be confined in pores of different sizes, or may be physically or chemically trapped in specific microstructures. T_1 decreases with the pore size, and other more subtle relationships may be found between the porous structure and relaxation times of water inside. This work focused on the development of pore structure over time due to the hydration of the binder, and it is evident that the technique is effective as a method of measuring pore size distribution in bio-aggregate composites. Figure 2.12 shows the distribution of water in water-hemp mixtures with differing water to hemp mass ratios, and clearly shows the typical bi-modal pore size distribution that is known to occur in hemp shiv.

Fig. 2.12 T_1 distribution for water-hemp mixtures after 18 h for different water to hemp mass ratios: (from bottom to top) 0.62, 0.86, 1.12, 1.37, 1.63, 1.89, 2.14, and 2.4 (Faure et al. 2012)



2.2.2 Other Methods

2.2.2.1 Mercury Intrusion Porosimetry

Mercury intrusion porosimetry (MIP) is a powerful technique which can be used to explore the structure of pores larger than about 3.5 nm. In MIP, the volume of liquid metal that penetrates a solid is measured as a function of applied pressure. Subsequent analysis is based on the capillary law governing liquid penetration into small pores. Since mercury is a non-wetting liquid for most materials (its contact angle is greater than 90°), an externally imposed pressure is required to force it into the pores of a porous solid.

The smaller the pore size, the greater the pressure required to force the mercury into the pore. In general, penetration data are analyzed using the Washburn equation (Washburn 1921). This relates the radius r of pores (assumed to be cylindrical) to the imposed pressure P as follows:

$$P = \frac{-2\gamma \cos \theta}{r}$$

where:

γ Interfacial energy (surface tension) of mercury

θ contact angle of mercury with the material

Common values of γ and θ (which assume interfaces involving a gas or vapour phase) are 485 mJ/m² and 140°. Whilst pores are rarely cylindrical, the Washburn equation is generally accepted as a practical method of analysing what are normally very complex pore systems (Lawrence 2007).

Boitryk and Pawluczuk (2014) have tested bio-composites (reed and sawdust bound with cement) using MIP in order to establish the impact of superplasticizer. Collet et al. (2008) tested hemp-lime renders and mortars using MIP. This study found that the pore size distributions of the composites were monomodal, with frequency peaks at about 0.9 μm . The vast majority of the pores seen were in the meso- and macro-pore range (respectively 96 and 94% of the intruded mercury volume). They also identified a significant hysteresis between the intrusion and extrusion curves. This was explained in part by the ‘ink-bottle’ effect where mercury became trapped in pores with smaller pore openings, and partly by a difference in the contact angle between intrusion and extrusion. In some cases hysteresis can be completely eliminated by modifying the extrusion contact angle (León 1998). It should be noted that a third cause could also be considered, associated with the crushing of pore walls. This would result in very different extrusion curves because the porosity would have been changed by the high pressures involved in intrusion.

Figure 2.13 shows pore size distributions obtained by Collet (2008) and Boitryk (2014) which differ significantly. Part of the difference is likely to be due to the different binders used, and potentially also due to differences in hemp shiv itself,

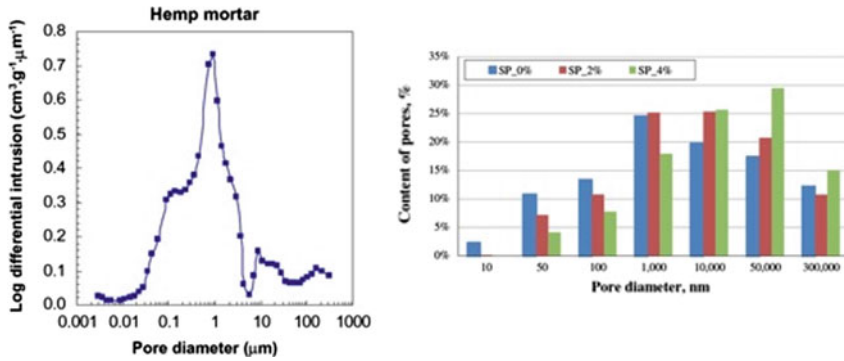


Fig. 2.13 Pore size distribution of hemp-lime composites using MIP. Collet (2008) left; Boitryk (2014) right

but it is evident that a more systematic study of the use of MIP to characterise the pore size distribution of bio-aggregates is required.

There do not appear to be any MIP studies of bio-aggregate on its own.

2.2.2.2 Thermoporometry

A small crystal of a liquid melts at a lower temperature than the bulk liquid, as given by the Gibbs-Thomson equation (Jackson and McKenna 1990). Thus if a liquid is imbibed into a porous material, and frozen, the melting temperature will provide information on the pore-size distribution. The detection of the melting can be done by sensing the transient heat flows during phase-changes using differential scanning calorimetry.

For an isolated spherical solid particle of diameter x in its own liquid, the Gibbs-Thomson Equation for the structural melting point depression can be written:

$$\Delta T_m(x) = T_{mB} - T_m(x) = T_{mB} \frac{4\sigma_{sl}}{H_f \rho_s x}$$

where:

- T_{mB} Bulk Melting temperature
- σ_{sl} solid-liquid interface energy (per unit area)
- H_f bulk enthalpy of fusion (per gram of material)
- ρ_s density of solid

Very similar equations may be applied to the growth and melting of crystals in the confined geometry of porous systems. However the geometry term for the crystal-liquid interface may be different, and there may be additional surface energy terms to consider, which can be written as a wetting angle term $\cos\phi$. The angle is

usually considered to be near 180° . In cylindrical pores there is some evidence that the freezing interface may be spherical, while the melting interface may be cylindrical, based on preliminary measurements for the measured ratio for $\Delta T_f/\Delta T_m$ in cylindrical pores (Webber 2010).

Thus for a spherical interface between a non-wetting crystal and its own liquid, in an infinite cylindrical pore of diameter x , the structural melting point depression is given by:

$$\Delta T_m(x) = T_{mB} - T_m(x) = -T_{mB} \frac{4\sigma_{sl} \cos \varphi}{H_f \rho_s x}$$

There has not been any published work which uses thermoporometry to characterize the pore structure of bio-based aggregates, although theoretically it should produce more representative results than MIP because it is conducted at atmospheric pressure which makes it less likely to crush pore walls during the characterization.

Landry (2005) has shown that Thermoporometry can be conducted using organic liquids as a probe, and cyclohexane is suggested to be a convenient organic liquid because its fusion temperature is 279.7 K (6.6 °C), very close to water. Cyclohexane is hydrophobic and non polar which would present a different interaction with the surface of the bio-aggregate than water. As a probe liquid, cyclohexane provides a complete baseline resolution at a 0.06 K/min scanning rate for all pore sizes. Another advantage to using hydrocarbons for thermoporometry characterisation of large pore materials is the larger temperature depression it offers compared with water.

2.2.2.3 Physisorption

The term “physical adsorption” or “physisorption” refers to the phenomenon of gas molecules adhering to a surface without the formation of a chemical bond at a pressure less than the vapor pressure. The attractions between the molecules being adsorbed and the surface are relatively weak and definitely not covalent or ionic. Some adsorption process is accompanied by absorption, which is the penetration of the fluid into the solid phase. It is sometimes difficult to distinguish between adsorption and absorption. This interaction is generally the result of a van der Waals interaction. On the other hand, chemical adsorption, called chemisorption, occurs when a molecule or atom is adsorbed to a surface by forming a chemical bond. Chemisorption is limited to monolayer coverage (Sing 1985; Forrest 2012; Condon 2006; Rouquerol 2014). Physical adsorption takes place on all surfaces and can form multiple layers under proper conditions. Chemisorption, however, is highly selective and only proceeds as long as the adsorptive can make direct contact with the surface. It is therefore a single-layer process. The enthalpy of chemisorption is

often much greater than that of physical adsorption. The physical sorption energy usually not exceed 80 kJ/mole, with typical energies being considerably less due to relatively weak Van der Waals's forces. Physically adsorbed molecules may diffuse along the surface of the adsorbent and typically are not bound to a specific location on the surface. Being only weakly bound, physical adsorption is easily reversed. A chemical bond involves sharing of electrons between the adsorbate and the adsorbent, with typical energies up to about 600 kJ/mole for C–N bonds and 800 kJ/mole for chemical bonds. Due to the bond strength, chemical adsorption is difficult to reverse (Webb 2003; Rouquerol 2014).

For physisorption, the principle measurement performed as an adsorption experiment is the measurement of the adsorption isotherm. The adsorption isotherm is the measurement of amount adsorbed versus adsorptive pressure at constant temperature. The slightest change in the shape of the plotted isotherm is indicative of a particular surface feature. Analyses of physical adsorption isotherm data reveal the total surface area, mesopore and micropore volume and area, total pore volume, the distribution of pore volume and area by pore size, and surface energy distribution. This is the easiest measurement to make. Another type of measurement is calorimetry. There are various forms of calorimetry but the most accurate methods are very difficult to perform and only a few examples are available in the literature. There are principal methods to measure the adsorption isotherm, volumetric and gravimetric. In both methods the adsorbent is held at a constant temperature, usually near or at the boiling point of the adsorptive. The amount adsorbed is measured in the case of the volumetric system by measuring the pressure change and comparing this to the expected pressure change if the adsorbent were absent. In the case of the gravimetric measurement the amount adsorbed is indicated by the mass gain. The most common measurement of the isotherm is volumetric method. This method has the advantage that it is simplest and relatively inexpensive. It has the disadvantage of a greater uncertainty in the results. A low cost alternative to the volumetric is the flow or carrier gas system. The disadvantage of this method is that the results are very uncertain and normally does not yield the isotherm. Generally, the gravimetric method is more accurate and precise, however such instrumentation is more expensive and requires a little more skill and patience to operation.

When a polar molecule is adsorbed on an ionic or polar surface various types of specific interactions may contribute to the adsorption energy. A useful general expression for the adsorption energy, E_0 , at very low surface coverage was first proposed by Barrer (1966) in the form of the sum:

$$E_0 = E_D + E_R + E_P + E_{F\mu} + E_{FQ}$$

in which E_D and E_R represent the non-specific dispersion and repulsion contributions and the terms E_P , $E_{F\mu}$ and E_{FQ} represent, respectively, the three types of specific contributions: the polarization, field-dipole and field gradient-quadrupole energies. The adsorbent-adsorbate interactions must be studied at very low surface coverage. It is only under these conditions that we can eliminate, or at least minimize, the adsorbate-adsorbate interactions. Calorimetry measures the temperature change as

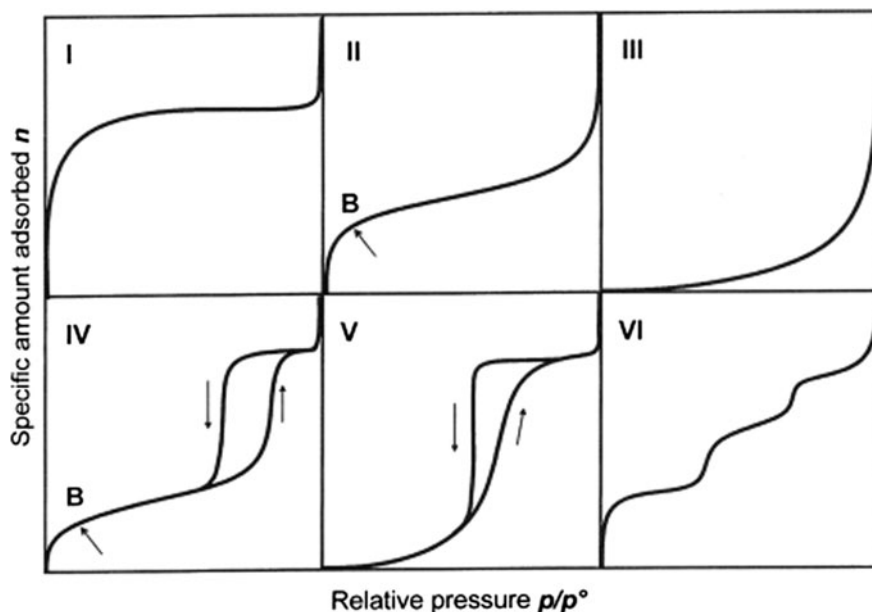


Fig. 2.14 The six main types of gas physisorption isotherms, according to the IUPAC classification (Sing et al. 1985)

the adsorption occurs. This along with a heat capacity measurements of the resultant adsorbate-adsorbent combination yields the heat of adsorption as a function of pressure. Calorimetry is not widely used since accurate calorimetry is extremely difficult to perform and requires a great amount of time and effort (Condon 2006).

Since physisorption is a complex process involving various interactions, the majority of these isotherms may conveniently be grouped into six classes in the IUPAC classification (Fig. 2.14).

- I: Microporous materials (e.g. Zeolite and Activated carbon)
- II: Non porous materials (e.g. Nonporous Alumina and Silica)
- III: Non porous materials and materials which have the weak interaction between the adsorbate and adsorbent (e.g. Graphite/water)
- IV: Mesoporous materials (e.g. Mesoporous Alumina and Silica)
- V: Porous materials and materials that have the weak interaction between the adsorbate and adsorbent (e.g. Activated carbon/water)
- VI: Homogeneous surface materials (e.g. Graphite/Kr and NaCl/Kr)

Several models have been developed to aid in the use of experimental data at the gas-solid interface. Each of these relies upon different assumptions that may affect the model's validity for a given surface. The Langmuir theory is used for ideal localized monolayer adsorption. The most widely used is the Brunauer, Emmett and Teller (BET) and its various modifications including the Brunauer, Deming,

Deming and Teller (BDDT). It is widely used for multilayer adsorption. The mechanisms involved in the BET model will be mainly dealt with next section. The calculation of the pore size distribution is performed by various methods based on the use of the Kelvin equation. Another widely used isotherm, especially for porous material, is the Dubinin-Radushkevich (DR) isotherm. Gibbs adsorption equation is to describe the adsorbed phase on available surface or in micropores. There are several other methods to describe the porosity, such as Barrett Joyner Halenda method (BJH), Density functional theory method (DFT) and Alpha S method (α_s) and so on (Sing 1985; Brunauer 1938; Condon 2006).

2.2.2.4 Nitrogen Adsorption and BET Analysis

Of all the many gases and vapours, which are readily available and could be used as adsorptive, nitrogen has remained universally pre-eminent. Nitrogen gas is generally employed as the probe molecule and is exposed to a solid under investigation at liquid nitrogen conditions (i.e. 77 K). The surface area of the solid is evaluated from the measured monolayer capacity and knowledge of the cross-sectional area of the molecule being used as a probe. For the case of nitrogen, the cross-sectional area is taken as $16.2 \text{ \AA}^2/\text{molecule}$. In the early 1930s, it was realized that multilayer adsorption of nitrogen can occur at liquid nitrogen temperature (77 K). Emmet and Brunauer came to the empirical conclusion that the beginning of the middle almost linear section of a Type II isotherm (Point B in Fig. 2.15) was the point most likely

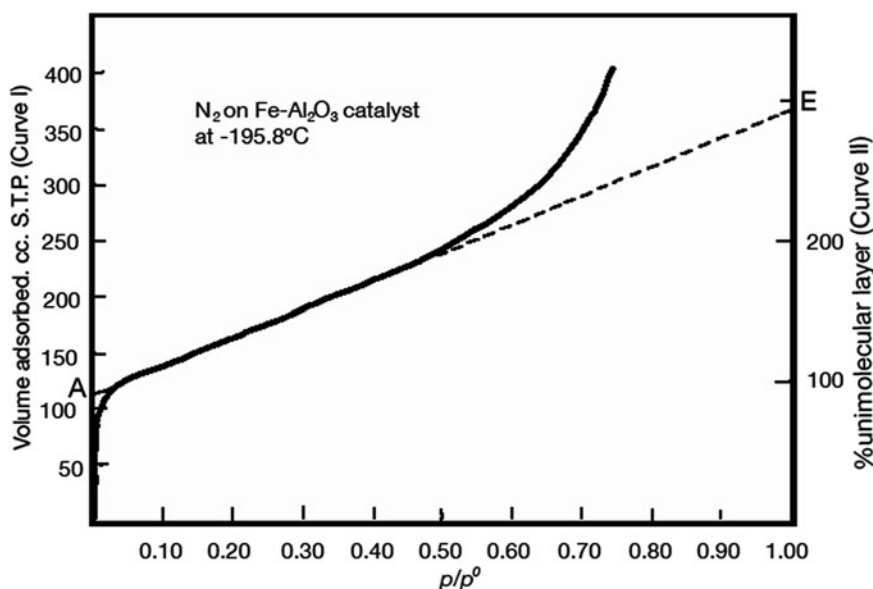


Fig. 2.15 Characteristic points on a Type II adsorption isotherm (Emmett 1937)

to correspond to monolayer completion. Their work prepared the way for the development of the BET theory in 1938. From the amount adsorbed at Point B, Emmett and Brunauer went on to calculate the surface area by assuming the monolayer to be molecularly close packed (Emmett 1937). To use of nitrogen adsorption for pore size analysis dates from the late 1940s. It is based on the application of the Kelvin equation, with a correction for the multilayer thickness on the pore walls. One of the computational method devised by Barrett, Joyner and Halenda (BJH) in 1951 remains the most popular way of deriving the pore size distribution from an appropriate nitrogen isotherm (Sing et al. 1998, 2001 and 2004).

Generally, two stages are involved in the evaluation of the surface area from physisorption isotherm data by the BET method. First, it is to construct the BET plot and to derive the value of the monolayer capacity, n_m . The second stage is the calculation of the specific surface area. The BET equation is conveniently expressed in the linear form:

$$\frac{p/p^0}{n(1 - p/p^0)} = \frac{1}{n_m C} + \frac{C - 1}{n_m C} \left(\frac{p}{p^0} \right)$$

where n ($=n^a/m^s$) is the amount adsorbed at a relative pressure p/p^0 and n_m ($=n^a/m^s$) is the monolayer capacity. In the BET theory, the parameter C is exponentially related to E_1 (the first-layer adsorption energy). A reliable analysis of the BET plot requires a certain number of experimental points: 10 is, we consider, a minimum in the exploratory range of relative pressures from 0.01 to 0.30. The location and extent of the linear region of a BET plot are dependent on the system and operational temperature, and if the isotherm is Type II or Type IV, the BET plot should always be located around the knee of the isotherm. The relative pressure corresponding to monolayer completion is inversely dependent on the C value, for example, if $C > 350$, the BET monolayer capacity is located at $p/p^0 < 0.05$ and if $C < 50$, n_m is at $p/p^0 > 0.18$. Point B cannot be identified as a single point on the isotherm. The selection of the appropriate pressure range often entails some degree of qualitative judgement and several narrow, adjacent, pressure ranges may seem to offer possible ranges of linearity. To overcoming this uncertainty, the following simple criteria have been proposed (Rouquerol et al. 2014): the range of linearity is restricted to a limited part of the isotherm—usually not outside the p/p^0 range of 0.05–0.30. It is strongly recommended that in reporting as (BET) values, the conditions of outgassing, the temperature of the measurements, the range of linearity of the BET plot, the values of p^0 , n_m^a , a_m and C should all be stated. Sing et al. (2001) pointed that, under favourable conditions, a t-plot can provide a means of assessing the micropore volume and the external area. The α_s method can be used to check the validity of the BET area and also to identify the adsorption and pore filling mechanism. In the absence of other complicating factors (e.g. microporosity or highly active sites), the BET plot of a type II or

type IV isotherm does appear to provide a fairly reliable assessment. It is not appropriate to apply the BET method to type III, type V or type VI isotherms. For a porous materials, or one that has an unsmooth surface, the BET surface area is generally appreciably larger than its non-porous analog. BET experiments are typically conducted to a relative pressure, P/P^0 , of approximately 0.3 at 77 K, where P^0 is the saturation pressure. At relative pressures above the point at which a N_2 monolayer has formed on the solid, capillary condensation occurs within the pore structure of the material such that the smaller pores are filled more easily and consecutively larger pores are filled as pressure is increased. When the saturation point is approached, i.e., P/P^0 is approximately 1.0, the internal pore structure of the material contains condensed (liquid) nitrogen. The total pore volume can be calculated by assuming that the density of liquid nitrogen in the pores is the same as that bulk liquid nitrogen. Nitrogen sorption is suitable to characterize materials with pores with the range of ~ 2 nm to below ~ 150 nm. For materials containing larger pores, mercury porosimetry is the preferred experimental technique and spans the pore range from 3.5 to 2000 nm. Sample preparation prior sorption analysis is a key aspect of material characterization. Caution must be used when heating some common samples because melting, dehydration, sintering, and decomposition are processes that can drastically alter the surface properties of the sample.

Collet et al. (2008) studied the porosity and pore structure of hemp wool, lime hemp render and hemp mortar by using BET methods with water vapour as probe agent. The results showed that the isotherms obtained are S-shaped and can be classified as type II according to IUPAC classification. The specific surface area for hemp mortar and hemp wool were 80.82 and 88.77 m^2/g , respectively. Collet et al. (2013) also showed that the isotherms of two kinds of hemp wool are classified as type II and the specific surface area is 111 m^2/g for the first hemp wool. Bismarck et al. (2002) showed all natural fibres have very small specific surface areas about 0.5 m^2/g , which is just slightly bigger than the calculated geometric surface area (As, geo 0.38 m^2/g at a fibre diameter $d_f \sim 14 \mu m$ (compare SEM-micrographs) and a density of flax fibres of $\rho = 1.47 g/cm^3$). Yin et al. (2015) compared the changes in micropore and mesopores in the wood cell walls of sapwood and heartwood. The results showed that specific surface area of sapwood ranged from 1.255 to 2.08 m^2/g , but specific surface area of heartwood ranged from 0.078 to 1.058 m^2/g . Brewer et al. (2014) that BET surface area of the slow pyrolysis biochars increased exponentially with pyrolysis temperature, from <1 to $317 \pm 16 m^2/g$ for the wood biochars and from $<1 m^2/g$ to $387 \pm 6 m^2/g$ for the grass biochars. BET surface area was low, $<10 m^2/g$, for all of the intermediate pyrolysis biochars. Rachini et al. (2012) showed the specific surface areas of natural, ethanol/water extracted and silane treated (at different concentrations) hemp fibres were about 0.7 m^2/g . Before BET characterization, the fibres (2 cm) were grounded onto very small pieces (500 nm) using a wood grinder.

2.2.2.5 Dynamic Vapour Sorption

Dynamic Vapour Sorption (DVS) is a gravimetric technique that measures the speed and amount of a solvent that is absorbed by a sample. It is an automated alternative to traditional sorption techniques. Within building materials the technique is primarily used to measure the sorption of water vapour, although using other solvents can provide some useful insights into pore structure and surface area.

Traditional water vapour sorption isotherms are conducted gravimetrically using saturated salt solutions which generate known relative humidity. For each humidity value, a sorption isotherm indicates the corresponding water content value at a given, constant temperature. If the composition or quality of the material changes, then its sorption behaviour also changes. Because of the complexity of sorption processes, the isotherms cannot be determined by calculation, but must be recorded experimentally for each product.

The main application of DVS is to measure water sorption isotherms. In general, a vapor sorption isotherm shows the equilibrium amount of vapor sorbed as a function of steady state relative vapor pressure at a constant temperature. For water sorption isotherms, water relative vapor pressure is more commonly expressed as relative humidity. In a DVS experiment this is accomplished by exposing a sample to a series of step changes in relative humidity and monitoring the mass change as a function of time. The sample mass must be allowed to reach gravimetric equilibrium at each step change in humidity before progressing to the next humidity level. Then, the equilibrium mass values at each relative humidity step are used to generate the isotherm. Isotherms are typically divided into two components: sorption for increasing humidity steps and desorption for decreasing humidity steps. Sorption can be further divided into adsorption (sorbate located on the surface) and absorption (sorbate penetrates the bulk). Figure 2.16 shows a typical DVS reference plot and isotherm for hemp-lime using water vapour. The chapter on hygric properties discusses sorption isotherms in detail and the extent to which they have been used with bio-aggregates

Figure 2.17 shows DVS data for hemp shiv using cyclohexane. This test allows an insight to be gained into the BET surface area and sorption kinetics as well as into porosity and diffusion. The cyclohexane sorption study (Fig. 2.17 up) on the sample indicates that there is a very small interaction between cyclohexane vapour and the hemp sample. The sorption isotherm (Fig. 2.17 down) shows the cyclohexane sorption capacity for hemp at 95% P/P^0 to be less than 1% by mass. The BET surface areas can be calculated from the BET model with cyclohexane as probe and give a specific surface area of 2.463 m²/g with a regression (R²) of linear fit of 99.846%. Table 2.2 shows that for the hemp shiv sample, for steps from 60% P/P^0 to 90% P/P^0 , there is a steady decrease in the diffusion constant almost linearly with increasing partial vapour pressures of cyclohexane. Although the hemp sample shows a straightforward sorption/desorption mechanism (Fig. 2.17 up), the isotherm (Fig. 2.17 down) shows a distinct Type IV mechanism with a characteristic hysteresis loop which can be associated with a mesoporous structure.

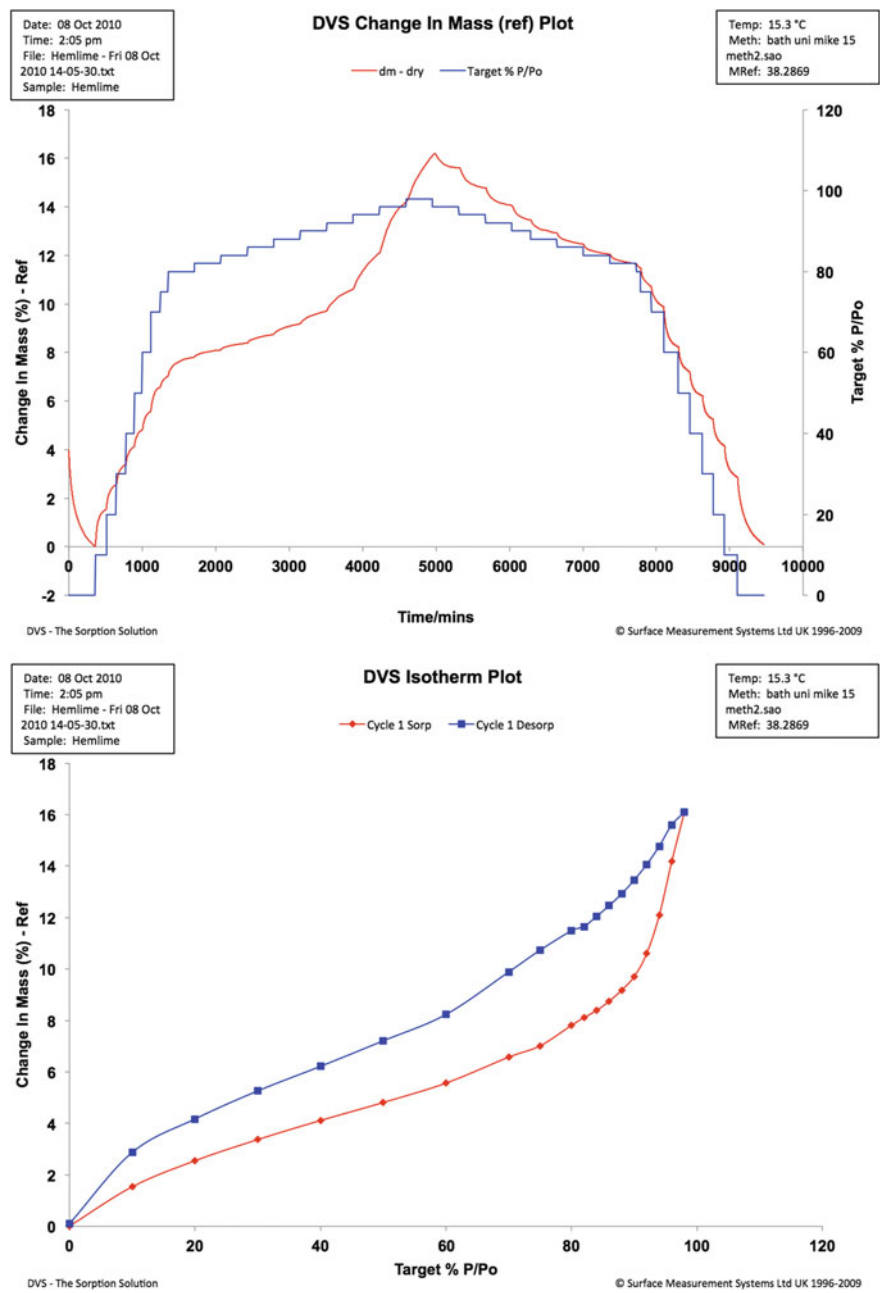


Fig. 2.16 Typical DVS reference plot (up) and sorption isotherm (down) for hemp-lime (author)

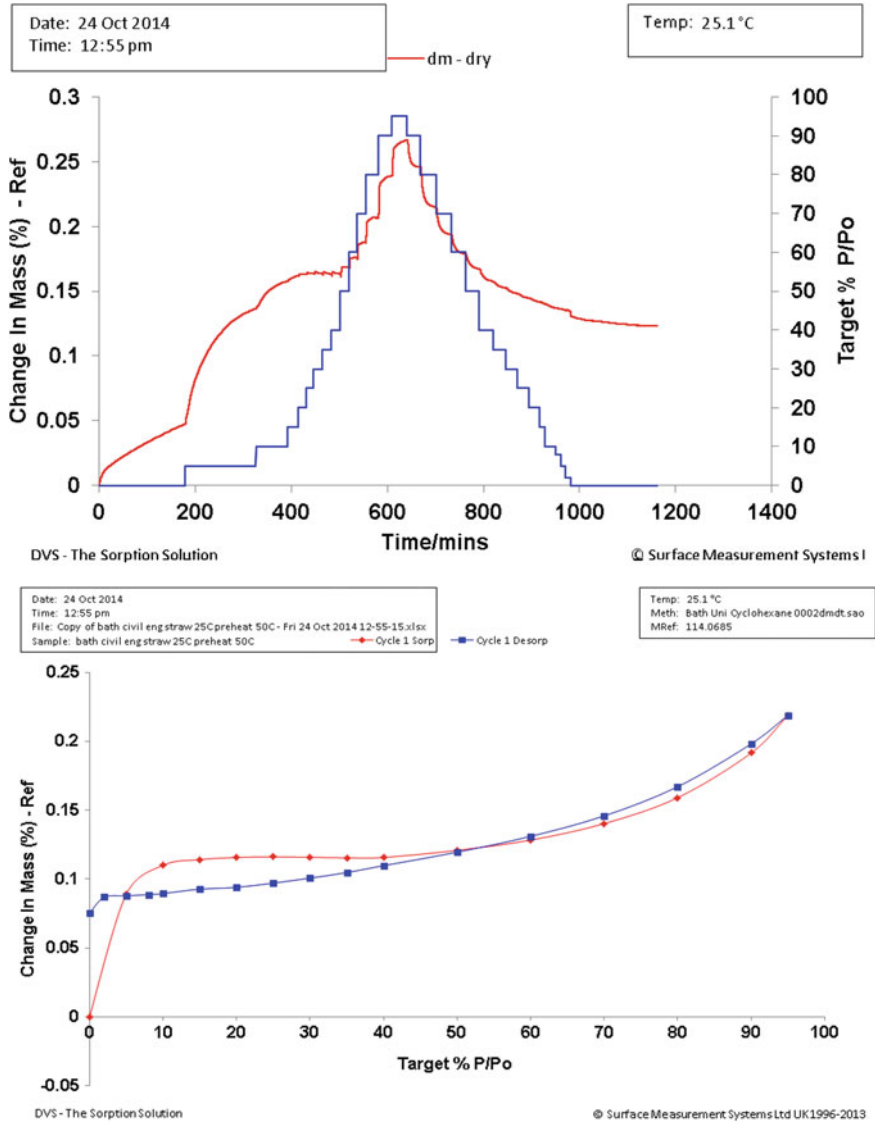


Fig. 2.17 DVS plots for hemp shiv using cyclohexane. Reference plot (*up*) and sorption isotherm (*down*) (author)

2.2.2.6 Pycnometry and Envelope Density Analysis

Pycnometry is used for measuring the density and the pore volume based on Boyle-Mariotte’s law of volume-pressure relationships. Details of the construction of simple gas pycnometers were published more than fifty years ago. There are

Table 2.2 Diffusion coefficients for hemp shiv sample

Hemp shiv			
Sample	%P/P ⁰	Temperature (°C)	Diffusion coefficient (cm ² /s)
Hemp	60–70	25.0	2.57E–04
Hemp	70–80	25.0	1.65E–04
Hemp	80–90	25.0	1.13E–04

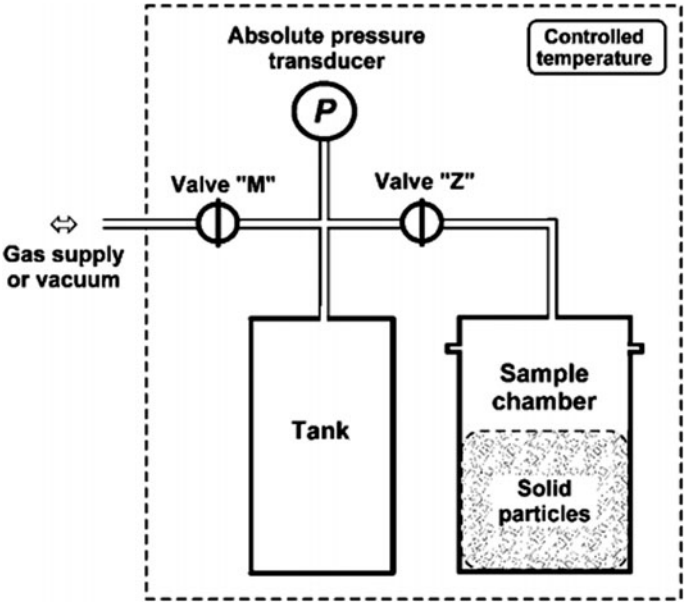


Fig. 2.18 Diagram of a constant volume gas pycnometer. The sample-chamber and the tank, initially filled with gas at two different pressures, are connected by opening vale ‘z’. The final gas pressure indicated of how much of the sample-chamber volume is occupied by the solid particles (Tamari 2004)

three kinds of gas pycnometers reported in literature: ‘constant-volume’, ‘variable volume’ and ‘comparative’ (Kummer 1945; Tamari 2004). The ‘constant-volume’ gas pycnometer was considered because of its widespread use. This technique uses the gas displacement method to measure volume accurately. As shown in Fig. 2.18, inert gases, such as helium or nitrogen, are used as the displacement medium. The sample is sealed in the instrument compartment of known volume, the appropriate inert gas is admitted, and then expanded into another precision internal volume. The pressures observed upon filling the sample chamber and then discharging it into a second empty chamber allow computation of the sample solid phase volume. Helium molecules rapidly fill pores as small as one angstrom in diameter; only the

solid phase of the sample displaces the gas. Dividing this volume into the sample weight gives the gas displacement density.

This method has been widely used to determine the volume and the density of bio-aggregates materials. Three fundamental hypotheses are made:

- (1) the gas inside the pycnometer behaves ideally (i.e. its compressibility is negligible and it does not adsorb on solids),
- (2) the sample and the pycnometer's components are rigid, and
- (3) the pycnometer is gas-tight and the expanding gas quickly reaches a static equilibrium.

The method consists of placing a dry core (or crushed rock) of known bulk volume (V_{bulk} , as determined by methods described above) in a container of known volume (V_a). This volume is connected with another container with a known volume (V_b) that is evacuated. He gas is introduced into V_a and the pressure (P_1) set to an arbitrary value typically around 100 psi. This He gas is then released into V_b and allowed to equilibrate throughout both chambers. The helium gas then penetrates into the pores of the sample. During this process the pressure will decrease to a new stable level (P_2). Using the ideal gas law, the volume of the pores can be calculated from

$$V_v = V_{bulk} - V_a - V_b \left(\frac{P_2}{P_2 - P_1} \right)$$

It must consider a range of possible values for the filling factor ($0 < \phi < 1$). The porosity of granular media lies between 25 and 50% in general, which would give the theoretical range $0.50 < \phi < 0.75$. However, in practice it would be difficult to fill the pycnometer's sample-chamber to the brim. We considered that 5–25% of the sample-chamber volume (including the tube at the sample-chamber side) might be free of solid particles. The range $0.40 < \phi < 0.70$ was thus thought to be realistic for a sample-chamber filled with as many solid particles as practical (Tamari 2004; Anovitz 2015). This method is recognized as one of the most reliable techniques for obtaining true, absolute, skeletal, and apparent volume and density. This technique is non-destructive as it uses the gas displacement method to measure volume. Inert gases, such as helium or nitrogen, are used as the displacement medium. Density calculations using the gas displacement method are much more accurate and reproducible than the traditional Archimedes water displacement method (Zauer et al. (2013).

Mwaikambo et al. (2001) studied the porosity of plant fibres by helium pycnometry method. The results showed that the porosity of hemp fibres is 2.46% and the porosity of Sisal and Jute are similar (10.85 and 11.36%, respectively). Zauer et al. (2013) studied porosity of wood by pycnometry method using helium and nitrogen as a displace gas. The results in Table 2.3 showed how this can lead to misinterpretation of the cell wall density or porosity of wood determined by gas pycnometry. The results clearly showed that the sample geometry and the dimensions

Table 2.3 Average cell wall densities and porosities of oven dry native spruce, maple and ash in dependence of sample dimension or geometry as well as displacement gas (helium and nitrogen) (Zauer et al. 2013)

Wood species	Thickness (mm)	Thickness direction	Helium		Nitrogen	
			Cell-wall density (g cm ⁻³)	Porosity (%)	Cell-wall density (g cm ⁻³)	Porosity (%)
Spruce	2	Long	1.47	71.4	1.40	70.3
		Tang	1.29	67.3		
	6	Long	1.38	69.9		
		Tang	1.31	67.4		
Maple	2	Long	1.51	65.8	1.46	64.7
		Tang	1.43	64.3		
	6	Long	1.43	64.0		
		Tang	1.40	63.1		
Ash	2	Long	1.36	52.2	1.35	51.3
		Tang	1.35	51.3		
	6	Long	1.32	50.4		
		Tang	1.33	51.1		

significantly affect the calculated values. This is primarily due to the inaccessibility of some uncut wood cell lumen. Thus, the determined cell wall volume is falsely too high, and consequently, the calculated cell wall density or porosity falsely too low.

Donato (2012) studied the porosity of waterlogged woods by using helium pycnometry. The porosity of waterlogged wood ranged between 83.4 and 90.6%. The author believed the porosity values calculated using the helium pycnometer are reliable because helium may easily penetrate even in the smallest cavities of the cell wall. Eventual differences between the porosity values obtained in wet and dry conditions might be ascribed to different structure assumed by the cell wall and different water and helium penetration, which is larger for the inert gas. Gershon et al. (2010) studied the porosity of light wood and dark using pycnometry method. This results in a volume fraction of porosity of 0.82 for the dark and 0.80 for the light.

2.3 Conclusion

There are a large number of methods for determining porosity. However, the porosity of bio-aggregates is difficult to quantify due to the complex pore size and shape. For example, the size of pore in the bio-aggregate are between a few nanometers to several millimeters. There is really no one method that can

characterize pores in this enormous range in scale. In this chapter, the theory, advantage and disadvantage of several common methods using for determination of porosity have been briefly described and summarised. In essence, the different techniques, each based on different inherent assumptions, have their own capabilities and advantages. A combination of several methods is most likely to give a good understanding of the size, shape and structure of pore in the bio-aggregates materials.

The study of bio-aggregates is still in its infancy and their unique characteristics demand the development of novel methods or the adaptation of existing methods in order to satisfactorily characterise their microstructure. There is a need for robust and comprehensive studies to be made into these materials in order that their performance can be satisfactorily modelled using Building Physics models to confidently predict the performance of dwellings constructed from these materials.

References

- Anovitz, L.M., Cole, D.R.: Characterization and analysis of porosity and pre structures. *Rev. Mineral. Geochem.* **80**, 61–164 (2015)
- Aydilek, A.H., ASCE, A.M., Oguz, S.H., ASCE, M., Edil, T.B.: Digital image analysis to determine pore opening size distribution of nonwoven geotextiles. *J. Comput. Civil Eng.* **16**(4), 280–290 (2002)
- Barrer, R.M.: Specificity in physical sorption. *Journal of colloid interface science* **21**, 415–434 (1966)
- Bismarck, A., Askargorta, I., Agranberri, S., Jurgen, L., Thomas, W., Bernhard, S., Artemis, S.I., Limbach, H.H.: Surface characterization of flax, hemp and cellulose fibers; surface properties and the water uptake behaviour. *Polym. Compos.* **23**(5), 872–894 (2002)
- Boitryk, M., Pawluczuk, E.: Properties of a lightweight cement composite with an ecological organic filler. *Constr. Build. Mater.* **51**, 97–105 (2014)
- Brewer, C.E., Chuang, V.J., Masiello, C.A., Gonnermann, H., Gao, X., Dugan, B., Driver, L.E., Panzacchi, P., Zygourakis, K., Davies, C.A.: New approaches to measuring biochar density and porosity. *Biomass Bioenergy* **66**, 176–185 (2014)
- Brunauer, S., Emmett, P.H., Teller, E.: Adsorption of gases in multimolecular layers. *J. Am. Chem. Soc.* **60**, 309–319 (1938)
- Chundawat, S.P.S., Donohoe, B.S., Sousa, L., da Costa, E., Thomas, A., Umesh, P., Lu, F., Ralph, J., Himmel, M.E., Balan, V., Dale, B.E.: Multi-scale visualization and characterization of lignocellulosic plant cell wall deconstruction during thermochemical pretreatment. *Energy Environ. Sci.* **4**, 937 (2011)
- Collet, F., Bart, M., Serres, L., Miriel, J.: Porous structure and water vapour sorption of hemp-based materials. *Constr. Build. Mater.* **22**, 1271–1280 (2008)
- Collet, F., Chamoin, J., Pretot, S., Lanos, C.: Comparison of the hygric behaviour of three hemp concretes. *Energy Build.* **62**, 294–303 (2013)
- Condon, J.B.: Surface area and porosity determinations by physisorption measurements and theory. Elsevier, Oxford (2006)
- Donato, I.D., Lazzara, G.: Porosity determination with helium pycnometry as a method to characterize waterlogged woods and the efficacy of the conservation treatments. *Archaeometry* **54**(5), 906–915 (2012)

- Dougal, A., Jerram, Kent, & Adam, J.R.: An overview of modern trends in petrography: textural and microanalysis of igneous rocks. *J. Volcanol. Geoth. Res.* **154**, 158 (2006)
- Dougal, A., Jerram, Higgins, & Micahael, D.: 3D analysis of rock textures: quantifying igneous microstructures. *Elements* **3**, 239–245 (2007)
- Emmett, P.H., Brunauer, S.: The use of low temperature van de Waals adsorption isotherms in determining the surface area of iron synthetic ammonia catalysts. *J. Am. Chem. Soc.* **59**(8), 1553–1564 (1937)
- Faure, P., Peter, U., Lesueur, D., Cossot, P.: Water transfers within Hemp Lime concrete followed by NMR. *Cem. Concr. Res.* **42**, 1468–1474 (2012)
- Forrest, S.C.: Physical adsorption of gases onto mesoporous silica material SBA-15. *Chemistry publications and other works* (2012)
- Gershon, A.L., Bruck, H.A., Xu, S., Sutton, M.A., Tiwari, V.: Multiscale mechanical and structural characterizations of Palmetto wood for bio-inspired hierarchically structured polymer composites. *Mater. Sci. Eng. C* **30**, 235–244 (2010)
- Grove, C., Jerram, D.A.: jPOR: an imageJ macro to quantify total optical porosity from blue-stained thin sections. *Comput. Geosci.* **37**, 1850–1859 (2011)
- Kain, G., Johann, C.P., Marius-Catalin, B., Bernhard, P., Klaus, R., Alexander, P.: Analyzing wood bark insulation board structure using X-ray computed tomography and modelling its thermal conductivity by means of finite difference method. *J. Compos. Mater.* **0**(0), 1–12 (2015)
- Hamdi, S.E., Delisee, C., Malvestio, J., Silva, N.D., Duc, A.L., Beaugrand, J.: X-ray computed microtomography and 2D image analysis for morphological characterization of short lignocellulosic fibres raw materials: a benchmark survey. *Compos. A* **76**, 1–9 (2015)
- Jackson, C.L., McKenna, G.B.: The melting behavior of organic materials confined in porous solids. *J. Chem. Phys.* **93**(12), 9002–9011 (1990)
- Kaestner, A., Lehmann, E., Stamparoni, M.: Imaging and image processing in porous media research. *Adv. Water Resour.* **31**(9), 1174–1187 (2008)
- Kummer, F.A., Cooper, A.W.: Soil porosity determination with the air pycnometer as compared with the tension method. *Agric. Eng.* **26**, 21–23 (1945)
- Landry, M.R.: Thermoporometry by differential scanning calorimetry: experimental considerations and applications. *Thermochim. Acta* **433**, 27–50 (2005)
- Latif, E., Lawrence, R., Shea, A., Walker, P.: Moisture buffer potential of experimental wall assemblies incorporating formulated hemp-lime. *Build. Environ.* **93**(2), 199–209 (2015)
- Lawrence, R.M., Mays, T.J., Rigby, S.P., Walker, P., D'Ayala, D.: Effects of carbonation on the pore structure of non-hydraulic lime mortars. *Cem. Concr. Res.* **37**, 1059–1069 (2007)
- León, C.A.L.: New perspectives in mercury porosimetry. *Adv. Colloid Interf. Sci.* **76–77**, 341–372 (1998)
- Lubelli, B., de Winter, D.A.M., Post, J.A., van Hees, R.P.J., Drury, M.R.: Cryo FIB SEM and MIP study of porosity and pore size distribution of bentonite and kaolin at different moisture contents. *Appl. Clay Sci.* **80**(81), 358–365 (2013)
- Maire, E.: X-ray tomography applied to the characterization of highly porous materials. *Annu. Rev. Mater. Res.* **42**, 136–178 (2012)
- Maire, E., Buffiere, J.Y., Salvo, L., Blandin, J.J., Ludwig, W., Letang, J.M.: On the application of X-ray microtomography in the field of materials science. *Adv. Eng. Mater.* **3**, 539–546 (2001)
- Manger, G.E.: Porosity and bulk density of sedimentary rocks. *Geol. Surv. Bull.* **114-E** (1963)
- Marinello, F., Bariani, P., Savio, E., Horsewell, A., De Chiffre, L.: Critical factors in SEM 3D stereo microscopy. *Measur. Sci. Technol.* **19** (2008)
- Mermut, A.R.: Historical development in soil micromorphological imaging. *J. Mountain Sci.* **6**(2), 107–112 (2009)
- Mostefai, N., Hamzaoui, R., Guessasma, S., Amadou, A.W., Nouri, H.: Microstructure and mechanical performance of modified hemp fibre and shiv mortars: discovering the optimal formulation. *Mater. Des.* **84**, 359–371 (2015)

- Mwaikambo, L.Y., Ansell, M.P.: The determination of porosity and cellulose content of plant fibers by density method. *J. Mater. Sci. Lett.* **20**, 2095–2096 (2001)
- Nimmo, J.R.: Porosity and pore size distribution. *Encycl. Soils Environ.* **3**, 2935–303 (2004)
- Phillipson, M.N., Baker, P.H., Davies, M., Ye, Z., McNaughtan, A., Galbraith, G.H., McLean, R. C.: Moisture measurement in building materials: an overview of current methods and new approaches. *Build. Serv. Eng. Res. Technol.* **28**(4), 303–316 (2007)
- Rachini, A., Le Troedec, M., Peyratout, C., Smith, A.: Chemical modification of hemp fibers by silane coupling agents. *J. Appl. Polym. Sci.* **123**(1), 601–610 (2012)
- Roche, R.C., Abel, R.A., Johnson, K.G., Perry, C.T.: Quantification of porosity in acropora pulchra (brook 1891) using X-ray micro-computed tomography techniques. *J. Exp. Mar. Biol. Ecol.* **396**, 1–9 (2010)
- Rouquerol, F., Rouquerol, J., Sing, K.S.W., Llewellyn, P., Maurin, G.: *Adsorption by Powders and Porous Solids Principles, Methodology and Applications*. Elsevier, Oxford (2014)
- Sassoni, E., Manzi, S., Motori, A., Montecchi, M., Canti, M.: Novel sustainable hemp-based composites for application in the building industry: physical, thermal and mechanical characterization. *Energy Build.* **77**, 219–226 (2014)
- Shen, W., Wan, J., Tokunaga, T.K., Kim, Y., Li, X.: Porosity calculation, pore size distribution and mineral identification within shale rocks: application of scanning electron microscopy and energy dispersive spectroscopy. *Electron. J. Geotech. Eng.* **20**, 11477–11490 (2015)
- Sing, K.S.W.: Reporting physisorption data for gas/solid systems with special reference to the determination of surface area and porosity (Recommendations 1984). *Pure Appl. Chem.* **57**(4), 603–619 (1985)
- Sing, K.: Adsorption methods for the characterisation of porous materials. *Adv. Colloid Interf. Sci.* **76–77**, 3–11 (1998)
- Sing, K.: The use of nitrogen adsorption for the characterisation of porous materials. *Colloids Surf. A* **187–188**, 3–9 (2001)
- Sing, K.: Characterisation of porous materials: past, present and future. *Colloids Surf. A* **241**, 3–7 (2004)
- Stevulova, N., Cigasova, J., Estokova, A., Terpakova, E., Geffert, A., Kacik, F., Singovszka, E., Holub, M.: Properties characterization of chemically modified hemp hurds. *Materials* **7**, 8131–8150 (2014)
- Tamari, S.: Optimum design of the constant volume gas pycnometer for determining the volume of solid particles. *Meas. Sci. Technol.* **15**, 549–558 (2004)
- Tran, L.Q.N., Minh, T., Nguyen, F., Fuentes, C.A., Chi, T., Truong, Vuure, Van, A.W., Verpoest, I.: Investigation of microstructure and tensile properties of porous natural coir fibre for use in composite materials. *Ind. Crops Prod.* **65**, 437–445 (2015)
- Walker, R., Pavia, S.: Impact of Hydration on the Properties of Hemp Lime Concrete. *Civil engineering research in Ireland CERAI*, Belfast (2014)
- Walker, R., Pavia, S., Mitchell, R.: Mechanical properties and durability of hemp-lime concretes. *Constr. Build. Mater.* **61**, 340–348 (2014)
- Washburn, E.W.: The dynamics of capillary flow. *Phys. Rev.* **17**, 273–283 (1921)
- Webb, P.A.: *Introduction to Chemical Adsorption Analytical Techniques and their Applications to Catalysis*. Technical publications, Micromeritics instrument corp (2003)
- Webber, J.B.W.: Studies of nano-structured liquids in confined geometries and at surfaces. *Prog. Nucl. Magn. Reson. Spectrosc.* **56**(1), 78–93 (2010)
- Williams, J., Lawrence, M., Walker, P.: Thermally modelling bio-composites with respect to an orientated internal structure. *Sustainable ecological engineering design for society*, Leeds, 17th–18th, September, 2015 (2015)
- Yang, B., Wu, A., Miao, X., Liu, J.: 3D characterization and analysis of pore structure of packed ore particle beds based on computed tomography images. *Trans. Nonferrous Met. Soc. China* **24**, 833–838 (2014)
- Yin, J., Song, K., Lu, Y., Zhao, G., Yin, Y.: Comparison of changes in micropores and mesopores in the wood cell walls of sapwood and heartwood. *Wood Sci. Technol.* **49**, 987–1001 (2015)

- Zauer, M., Pfriem, A., Wagenfuhr, A.: Toward improved understanding of the cell wall density and porosity of wood determined by gas pycnometry. *Wood Sci. Technol.* **47**, 1197–1211 (2013)
- Zhao, H., Darwin, D.: Quantitative backscattered electron analysis of cement paste. *Cem. Concr. Res.* **22**(4), 695–706 (1992)
- Ziel, R., Haus, A., Tulke, A.: Quantification of the pore size distribution (porosity profiles) in microfiltration membranes by SEM, TEM and computer image analysis. *J. Membr. Sci.* **323**, 241–246 (2008)

<http://www.springer.com/978-94-024-1030-3>

Bio-aggregates Based Building Materials
State-of-the-Art Report of the RILEM Technical
Committee 236-BBM

Amziane, S.; Collet, F. (Eds.)

2017, XXXIII, 263 p. 128 illus., 127 illus. in color.,

Hardcover

ISBN: 978-94-024-1030-3